ISSN 1846-6168 (Print), ISSN 1848-5588 (Online)
https://doi.org/10.31803/tg-20250115224222

Original scientific paper
Received: 2025-01-15, Accepted: 2025-02-21

Time Dependent Load Capacity of the Press Fit

Vinko Močilnik, Nenad Gubeljak*, Jožef Predan

Abstract: This study investigates the loading capacity of a press fit using experimental, numerical and theoretical methods. Tests on specimens with different interferences showed that the loading capacity increases over time as long as the plasticity remains at the micro level. At larger interferences, the plasticity extends to the macro level, which in the long term means a reduction in the loading capacity of the press fit due to creep. Numerical simulations using finite element modelling showed the influence of surface roughness and time-dependent effect on contact pressure and friction. Models in text books do not take in account plasticity and creep of the material in press fit. The phenomenon can lead to a weakening of the press fit over time. The results highlight the importance of optimizing the interference and surface preparation to improve the loading capacity and joint performance. The article presents an approach for calculating the press fit taking in to account the Bowden Tabor friction model and the visco-plasticity of the material used.

Keywords: FEM analysis; interface oversize; hub; shaft; loading creep; press fit; roughness

1 INTRODUCTION

A press fit is commonly used in engineering structures to connect a shaft and a hub. The parts fit together due to a radial pressure that depends on the amount of interference at the diameter where both parts touch. The two parts (shaft and hub) are permanently joined as a solid unit. Although interference is an effective way to transmit large torques, its disadvantage is that in some cases disassembly is very difficult or impossible, Fig. 1.

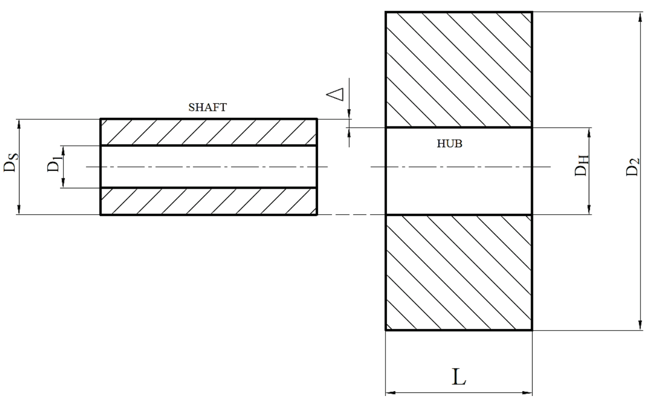

Figure 1 Basic principle of the press fit (D_1 – inner diameter of the shaft, D_S – nominal diameter of the shaft, D_H – nominal diameter of the hub, D_2 – external diameter of the hub, L – length of the press fit, Δ – interference of the press fit)

The composition of the such produced parts is possible in two ways:

a) By pressing the shaft into the hub.
b) By heating the hub or/and cooling the shaft to create a clearance between both parts.

The assembly of them is very simple and does not require a large assembly force. When the temperature, when the shaft be inserted, is gradually equalized, both parts want to return to their original dimensions and thus crash into each other; a pressure is created between them.

Due to the contact pressure at the nominal diameter, friction is established between the both parts, which resists against external forces in the axial and/or tangential direction. The greater the friction force, the greater the load capacity of the press fit. The average contact pressure along the joint and thus also the friction force depends on the size of the interference and the stiffness of the shaft and hub. The relationship between pressure and interference is linear if we assume that the material remains in the elastic region.

Lewis and co-workers in [1] measured the contact pressure in the varicose vein by using an ultrasound method to measure it. He showed that there is a region of uniform pressure within the contact zone and that on each side of the contact zone the contact pressure increases sharply. The average pressure along the length of the kink fits well with the results of the Lamé analysis, which is based on the plane stress state with considerable simplifications.

He concluded that the pressure distribution along the contact zone is comparable whether it is press fit.

Madej in [2] carried out the calculation of the interference fit with FEM analysis and compared the results with the experiment. He proved that the use of Lame's analysis gives a deficient estimation in some cases. The difference in the loading capacity of the interface fit can be up to 20 %. He showed that for accurate modelling it is necessary to use the size of the finite element less than 1% of the diameter of the axle. Autor's assessment is that in a more accurate analysis it is also necessary to model the friction. The Coulomb friction model is not sufficient to describe high-pressure sliding contact. The author suggests using the Bay-Wanheim (1976) model, which relates the frictional stress to the contact pressure.

In [3], the authors state that the force of static friction determines the strength of many different types of joints that are exposed to high loads, such as press-fits. The coefficient of static friction depends on many parameters, such as the mechanical properties of both materials, surface roughness, lubrication, impurities, hardness of contact surfaces, duration of contact and so on. In engineering calculations, the mean value of the coefficient of static friction, which is determined experimentally, is used. In order to determine the appropriate coefficient of static friction in a given case, a lot of experimental work is required. In order to simplify the process of determining the coefficient of static friction, the authors proposed a new calculation procedure based on the mechanical-molecular theory of friction. The results were compared with experimentally determined values and a sufficiently accurate match was found.

In [4], the author discusses the influence of surface roughness on the design of interference fits. It gives a detailed study of the influence of the surface roughness on the loading capacity of the interference fits. Here, the aspect of plastic deformation is neglected.

The authors in [5] and [6] measured the deformation of the bushing circumference using strain gauges on the outer diameter of the bushing. This then allowed them to estimate the contact pressure using analytical equations.

Croccolo et al. in [7] found that at interference fits between aluminium and steel, the coefficient of friction for dry aluminium-steel surfaces is 0.46. They developed an analytical model and reported that if the stiffness of both parts is close, the actual interference is likely to be less than the estimated interference. Mori et al. [8] analysis plastic deformation in press fit too. They recognized that the joining strength may be increased by forming beads and dimples. An example of the second type occurs when workpieces are mechanically interlocked by plastic deformation. An example of the second type occurs when the workpieces are mechanically connected by plastic deformation.

Yang et all in [9] point out that the optimum pressure between the two parts is reached only before the ring begins to plastically yield and that any further increase in the deformation pressure results in a negligible increase in the interference pressure and joint strength. That it is possible to increase joint strength by increasing the surface roughness or cleaning the contact surfaces.

The authors in [10] emphasize the importance of surface roughness in interference fit and demonstrate experimentally that the extraction load varies by up to 300 % for *Ra* values of 0.24 to 6.82 microns. They used an elastic two-dimensional model to model surface asperities on both the pin and bushing and report that despite high stresses that tend to crush the asperities, they tend to persist under high pressure. The authors in [11] analysed the interference fit of ring gear and stepped shaft using numerical and analytical methods and concluded that the Lame's equations underestimate the contact pressure by up to 78 %. The author in [12] used an analytical model to show that contact pressure varies with temperature; an increase in temperature leads to a decrease in the yield stress, which causes plastic deformation in the interference fit, thus reducing its loading capacity. Numerical methods were used to predict the quality of the joint. The author in [13] compared the load transfer at different values of interference and concluded that the use of a carefully selected interference, increases the durability of the joint.

2 MATERIAL PROPERTIES AND TESTING SPECIMEN

Eight test specimens of the press fit with different interferences were made eighteen years ago, with the aim of establishing the agreement between the results of the load capacity calculation of the press fit and the realistically measured values. The dimensions of the specimen are shown in Fig. 2. The inside of the hub was finely turned, the shaft was grinded. Assembly was carried out using the hub heating from 150 up to 450 °C in furnace, while shaft was at room temperature +20 °C. The smallest interference was 0.015 mm and increased up to 0.15 mm. The test specimens were loaded in the axial direction until the shaft began to slide in the hub. The maximum force was measured; the load capacity of the press fit. As the interference increased, it was to be expected that the load capacity of the press fit would also increase.

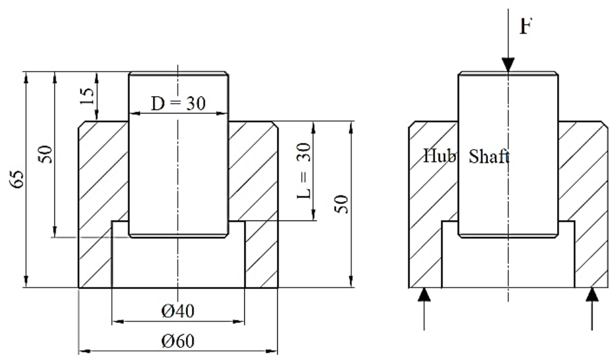

Figure 2 Specimen of press fit

S355 material with the following mechanical properties was used:
- Young's modulus E = 206 GPa
- Poisson's ratio v = 0.3
- elastic limit Re = 357 MPa
- tensile strength Rm = 512 MPa.

2.1 Rate-dependent Plasticity Creep Behaviour

A creep test of the material at constant stress was carried out. Fig. 3 shows setup for creep tension testing with elongation measurement at the INSTRON 1255 servo-hydraulic testing machine. Fig. 4 shows the white points at which the relaxation was measured. The three tensile test pieces were loaded to a white stress point and then keeping under constant plastic strain. The plastic strain was measured using an extensometer, and the moment when the stress was reached was considered as the time zero. Fig. 5 shows the dependences of the creep strain rate on time at constant stress. Three points 327 MPa, 398 MPa and 452 MPa were considered. Parameters A, n, and m were experimentally determined for ABAQUS FEM calculations.

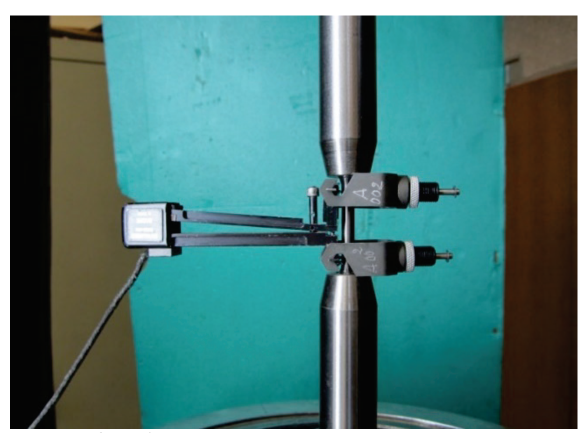

Figure 3 Setup for creep tension testing with elongation measurement

Fig. 4 shows the true stress-strain curve for this material in plastic range.

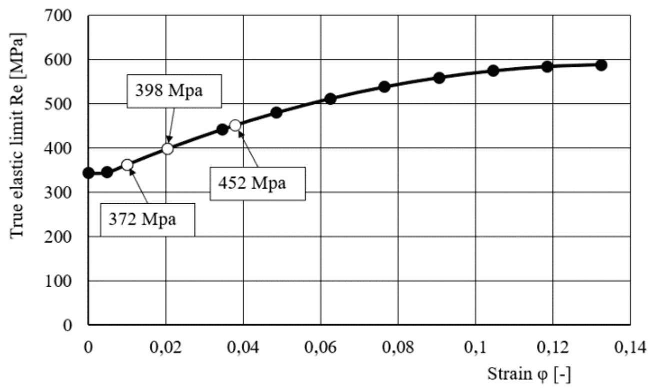

Figure 4 Tensile characteristic of the material S355 in plastic range

$$\dot{\varepsilon} = A \cdot \sigma^n \cdot t^m, \tag{1}$$

where: $\dot{\varepsilon}$ – uniaxial equivalent creep strain rate; σ – uniaxial equivalent deviatoric stress; A, n, m – constants determined experimentally at room temperature.

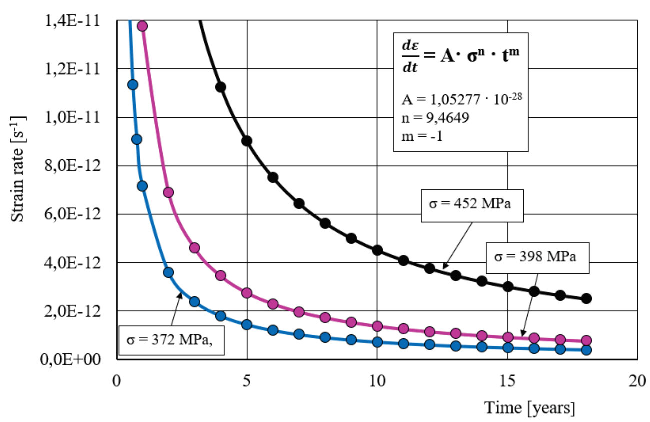

Figure 5 Time dependent properties of the used material

3 THEORETICAL BACKGROUND
3.1 Engineering Calculations

In literature for mechanical engineers, such as Decker [18] and Nieman [19], the procedure for calculating the press fit load capacity is described. The calculation is based on a theory that deals with stresses in a two-layer ring with the assumption of axial symmetry and a plane stress state, in elastic state of material.

The problem is solved using the first Lamé equation, written in the polar coordinate system, without considering volume forces, at a homogeneous temperature field, and has a form as follows:

$$\frac{\partial^2 u}{\partial r^2} + \frac{1}{r} \cdot \frac{\partial u}{\partial r} - \frac{u}{r^2} = 0. \tag{2}$$

The variable u is the displacement in the radial direction $u = u(r)$. Using $u = r^k$, where k is parameter, gives the general solution of the differential equation:

$$u(r) = Ar + Br^{-1}, \tag{3}$$

where A and B are integration constants. Using Hooke's Law:

$$\begin{aligned} \sigma_r &= \frac{E}{1-\nu^2}\left(\varepsilon_r + \nu\varepsilon_\varphi\right) = \frac{E}{1-\nu^2}\left(\frac{\mathrm{d}u}{\mathrm{d}r} + \nu\frac{u}{r}\right), \\ \sigma_\varphi &= \frac{E}{1-\nu^2}\left(\varepsilon_\varphi + \nu\varepsilon_r\right) = \frac{E}{1-\nu^2}\left(\frac{u}{r} + \nu\frac{\mathrm{d}u}{\mathrm{d}r}\right), \end{aligned} \tag{4}$$

can be written:

$$\begin{aligned} \sigma_r &= \frac{E}{1-\nu^2}\left[A(1+\nu) - \frac{B}{r^2}(1-\nu)\right], \\ \sigma_\varphi &= \frac{E}{1-\nu^2}\left[A(1+\nu) + \frac{B}{r^2}(1-\nu)\right], \end{aligned} \tag{5}$$

where σ_r in σ_φ are principal stress components in polar coordinate system.

In Eqs. (4) and (5), the designations mean: σ_r – stress in radial direction; σ_φ – stress in tangential direction (hoop stress); E – modulus of elasticity and ν – Poisson's ratio.

Eqs. (5) are written separately for the inner ring (shaft) denoted by I and for the outer ring (hub) denoted by II. This gives us four integration constants, which are calculated from the following boundary conditions:

a) $r = D_1/2 \rightarrow \sigma_r^{\mathrm{I}} = 0,$

b) $r = D/2 \rightarrow \sigma_r^{\mathrm{I}} = \sigma_r^{\mathrm{II}} = -p,$

c) $r = D/2 \rightarrow u^{\mathrm{II}} - u^{\mathrm{I}} = \Delta,$

d) $r = D_2/2 \rightarrow \sigma_r^{\mathrm{II}} = 0.$

where p - interference pressure and Δ – interference.

For the case, when $D_1 = 0$, can be used $\sigma_r(r) = \text{const.} = \sigma_r(r = D/2)$.

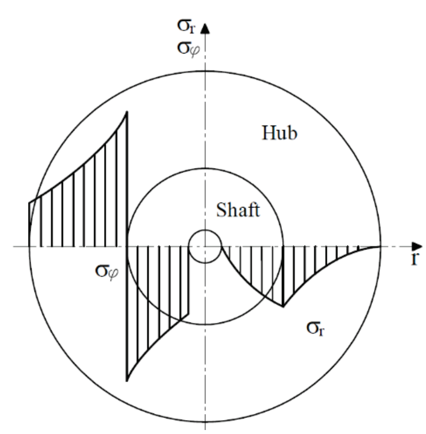

Figure 6 Elastic radial σ_r and tangential σ_φ stresses distribution on macro level of the press fit

The hub presses on the shaft due to elastic action as a spring. At larger interference, plastic deformation of the hub partially occurs, which could reduce the pressure between hub and shaft. This can happen if the plastic strain penetrates too deep into the material. Fig. 6 shows the elastic stress distribution on macro level of the press fit.

3.2 Coefficient of Static Friction at Large Pressure According to the Bowden-Tabor Model

The contact area, which is limited by the circumference at the nominal diameter and the length of the press fit, is called the apparent contact area. Due to the rough surface of the shaft and the hub, only some of the highest roughness peaks are in contact, which form the real contact area, which is one of the contact properties of the press fit at the micro level. The real contact area of the press fit increases with increasing normal force and is independent of the apparent contact area, [14]. This influence is not covered by the classic Coulomb law of sliding friction. The static coefficient of sliding friction can be significantly different on finely polished surfaces than on a realistic surface processed by turning and/or grinding. It should be emphasized that the roughness, both technologically and in terms of friction, must be in the optimal range, as described in [15] and [16].

The theory of the kinetic friction between two pure metal surfaces according to Bowden-Tabor [17] is based on the cold-press junction. At the points, at micro-level, where the two bodies are in touch, the surface of both, due to the great pressure, come so close together that a solid metallic bond is formed. Due to the pressure, the peaks on the rough surface deform plastically, new points come into contact and the contact surface increases. The oxide layer breaks down, impurities are squeezed out and a pure metal contact is formed. Cold pressed points at micro-contact are called contact area bridges. Under high pressure material plasticization, stress relaxation over time occurs, so the contact area bridges are enlarged and press fit load-capacity increases over time. As shown in this study, the load capacity increases with time only as long as the interference is small enough. However, with larger interferences, plasticization penetrates deeper into the shaft and bushing material and the opposite effect occurs; load capacity decreases. For pure metals without lubrication, strong adhesion and high normal force, the coefficient of static friction, according to the Bowden-Tabor, is approximated as:

$$\mu_0 \approx \frac{1}{\sqrt{3}} \cdot \left(\frac{2}{3-\xi} \right), \tag{6}$$

where ξ is so called Bowden-Tabor coefficient; in generally $\xi < 3$. In the case of $\xi = 0$ to 2.35, the coefficient of static friction is $\mu_0 = 0.4$ up to 1.8 [14].

4 SURFACE ROUGHNESS MEASUREMENT

With the help of a microscope KEYENCE VHX-7000, the roughness of the contact surface of the shaft and the hub was measured. The contact surface of the hub was turned to *Ra* 2.38 µm, and the contact surface of the shaft was ground to *Ra* 0.43 µm. Fig. 7 shows the image of both contact surfaces, and Fig. 8 shows the surface roughness profile for the shaft and the hub at reference length of 800 µm in initial contact.

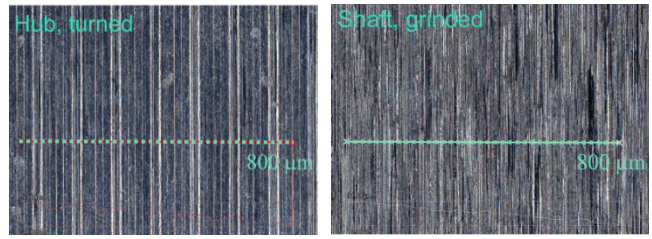

Figure 7 Surface image at reference length of 800 µm for shaft and hub

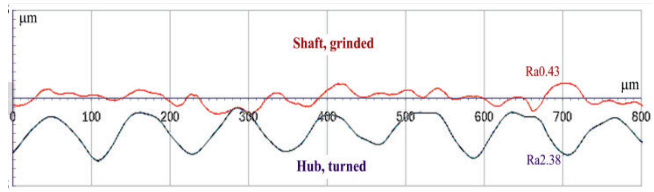

Figure 8 Surface roughness profile for the shaft and the hub at reference length of 800 µm in initial contact

At initial contact the roughness profile of the contact surface on the hub is deeper and periodically repeated, while the roughness profile of the ground shaft is shallower and random, Fig. 8.

5 FEM ANALYSIS

Fig. 9 shows the FEM analysis of the modelled contact roughness under a specified initial pressure. Contact bridges at micro-level and plasticization are visible.

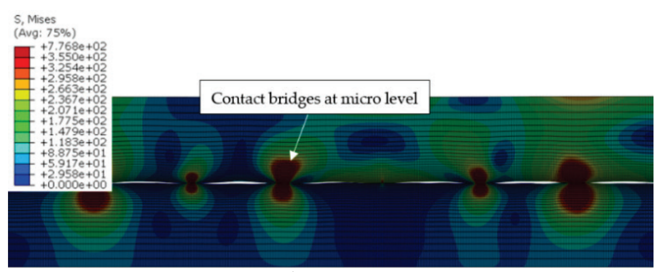

Figure 9 FEM analysis of the modelled roughness in contact

The numerical simulation of the stress-strain state in contact was performed using the software package SIMULIA Abaqus 2024. An elastic, plastic, and visco-plastic material behaviour model was employed. A hard contact model with a friction coefficient of 0.4 was used for modelling the contact. This approach allowed us to simulate material yielding around the contact area and stress relaxation over time due to material creep. In the linear elastic region, the Young's modulus was 206 GPa and Poisson's ratio was 0.3. The material has a yield strength of 357 MPa and strain-hardens to 591 MPa. A simple model accounting for time-dependent hardening was used for creep, with physical constants for this model experimentally determined as A = 1.05277e-28, n = 9.4649, and m = –1. The geometry was represented as a plane axisymmetric model. In the contact region, finite elements were refined to capture the relatively complex profile of the measured surface; nevertheless, the simulation required 556800 CAX4 type finite elements to describe the shaft and hub. The model was constrained in a way that allowed it to deform freely. Due to micro-plasticization in contact bridges, additional time-dependent plasticization occurs.

6 RESULTS AND DISCUSSIONS

The load capacity of the press fit was measured as a function of the interference, at the beginning immediately after assembly and after 18 years. The test results are collected in Tab. 1 and shown on the graph in Fig. 10. In addition to the measurement of the load capacity of the press fit, a calculation based on the linear theory of elasticity was performed for comparison, as presented in chapter 3. At the calculation, the coefficient of static friction $\mu_0 = 0.2$ has been taken in account, in accordance with the recommendations from the literature Decker [18] and Nieman [19].

The results of the test of the load capacity of the press fit, depending on the interference, show that the actual load capacity is much higher than the calculated one. With time, the load capacity of the press fit increases to an interference of 0.05 mm, after which a noticeable drop in the load capacity is detected with respect to the initial state.

Table 1 Measured and calculated load capacity of the press fit

Δ (mm)	Measured load capacity F_M (kN)	Load capacity after 18 years F_M (kN)	Calculated load capacity F_C (kN), $\mu_0 = 0.2$	Integration constant A	Integration constant B
0.015	66.1	181.12	22.2	4.10e-5	0.075
0.030	124.5	177.16	44.5	8.38e-5	0.150
0.045	167.8	182.37	66.8	1.25e-4	0,224
0.060	233.4	190.0	89.1	1.67e-4	0,299
0.075	288.1	211.26	111.4	2.09e-4	0.374
0.085	326.1	220.0	126.2	2.37e-4	0.424
0.100	384.1	198.0	148.5	2.79e-4	0.498
0.115	410.5	145.97	170.7	3.21e-4	0.573

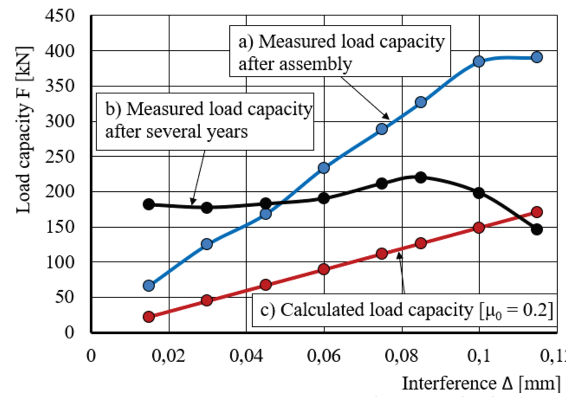

Figure 10 Measured and calculated load capacity of the press fit: a) Measured load capacity after assembly; b) Measured load capacity after 18 years; c) Calculated load capacity, using linear elastic theory of Lamé, and $\mu_0 = 0.2$

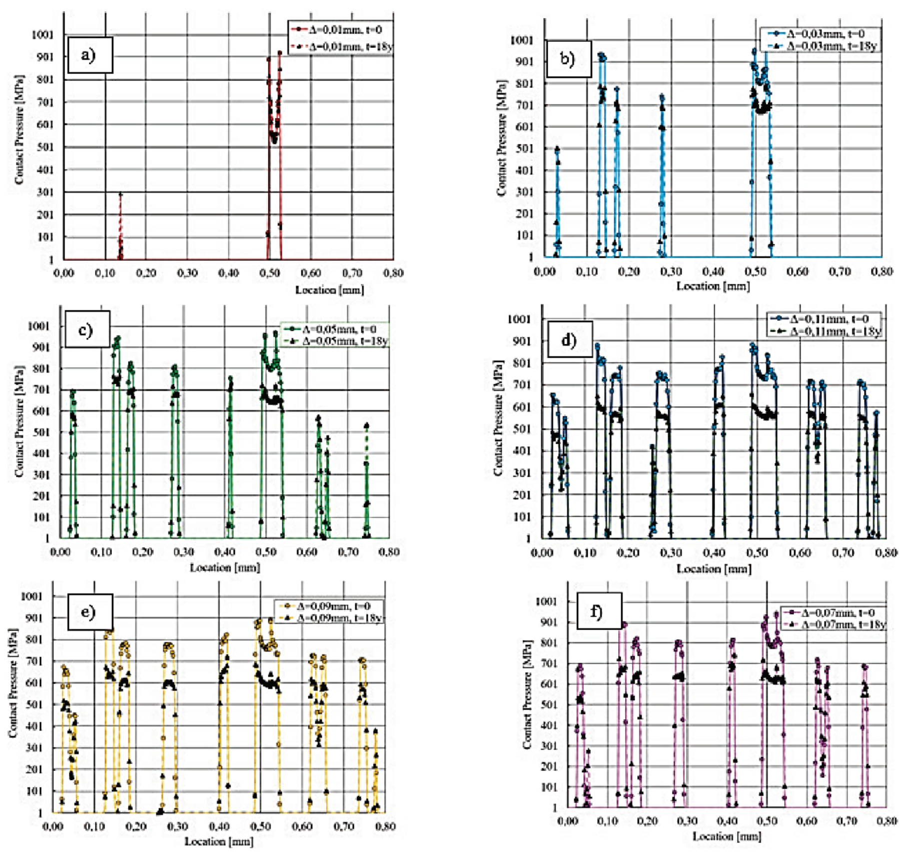

Figure 11 Numerical calculated contact pressure at reference length of 0,8 mm of contact surface at assembly, $t = 0$, and after 18 years, $t = 18y$ in dependence on interference Δ: a) Δ = 0.01 mm; b) 0.03; c) 0.05; d) 0.07; e) 0,09 and f) 0.11 mm.

Fig. 11 from a) to f) shows the results of the numerical analysis of the contact pressure for interferences from 0.01 to 0.11 mm at a reference contact length of 0.8 mm, immediately after assembly and after the passage of 18 years. The numerical analysis includes an elastic-visco-plastic material model. With increasing interference, the number of contact bridges increases, and also real contact area on the micro level. As the interference enlarges, the contact pressure on the real contact area also increases, the material plasticizes there, and with time stress relaxation occurs, which can be seen in Fig. 12 as a drop in the contact pressure during time.

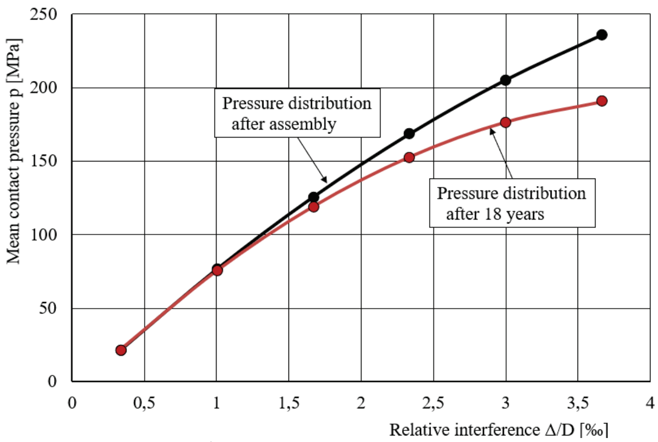

Figure 12 Distribution of the mean contact pressure in dependence on relative interference *Δ/D*

Fig. 12 shows the distribution of the mean contact pressure as a function of the relative interference, immediately after the mechanical joining of the press fit and after 18 years. The curves are a summary of the FEM analysis results from Fig. 11. Up to a relative interference of 1.6 ‰, there is no significant drop in contact pressure, while at larger relative interferences the drop in the contact pressure is greater due to stress relaxation of the plasticized material.

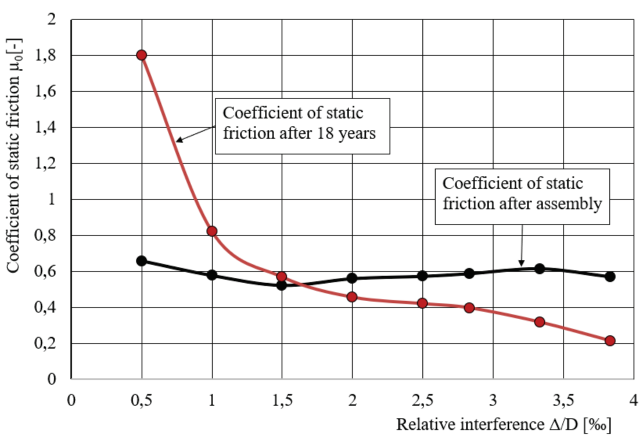

Figure 13 Distribution of the coefficient of static friction in dependence on relative interference *Δ/D* at the apparent contact area

Based on the numerically calculated mean contact pressure and the measured load capacity of the press fit, the coefficient of static friction on the apparent contact area was calculated. Fig. 13 shows the distribution of the coefficient of static friction μ_0 in dependence on relative interference of the press fit. After assembly, the mean coefficient of static friction was around 0.6, while after 18 years the coefficient of static friction is very variable and amounts to μ_0 = 1.8 for a relative interference of 0.5 ‰ and 0.2 for a relative interference of 3.83 ‰.

Fig. 14 shows the distribution of the Bowden-Tabor coefficient ξ in dependence on relative interference of the press fit. The coefficient ξ was calculated based on Eq. (6). At the beginning, the value of the coefficient was around 1, while after 18 years, the value of this coefficient changes from ξ = 2.36 for a relative interference of 0.5 ‰ to ξ = –2.42 for a relative interference of 3.83 ‰.

In any case, regardless of the size of the interface, plasticization of the material occurs due to the high pressure and the small actual contact area. With a relative interference of up to 1.6 ‰, the pacification of the material is at the micro level, which means that only the peaks of the roughness of the actual contact area are plastically deformed, which increases as a result. Due to the cohesive forces, the two materials in contact are cold pressed and very strong contact bridges are formed. Over time, creep of the material occurs and the contact bridges become even stronger. The contact pressure does not decrease, because creep occurs only at the micro level. The outer layers of the material remain in the elastic range and act as a spring at all times, maintaining the contact pressure.

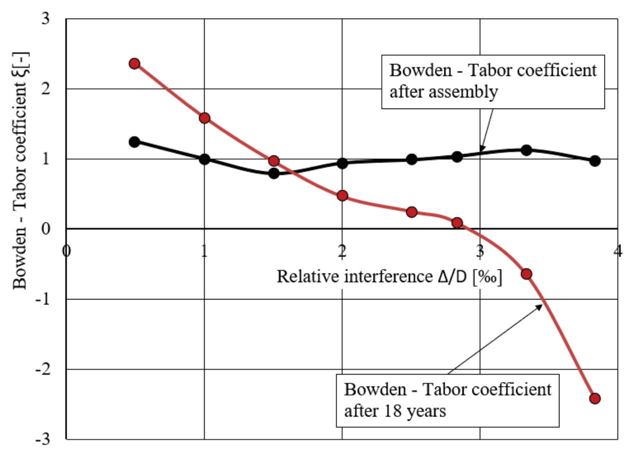

Figure 14 Distribution of the Bowden – Tabor coefficient ξ in dependence on relative interference Δ/D at the apparent contact area

Fig. 15 shows an equivalent creep strain, and Figure 16 shows an equivalent plastic strain in dependence on interference. At interference above 0.05 mm, plasticization extends to the macro level, which causes more intensive creep of the material in the hub. Contact pressure, the coefficient of sliding friction, and consequently the load capacity of the press fit decrease.

At an interference above 1.6 ‰, plasticization penetrates deeper into the material at the macro level, Figs. 15 and 16. In the initial state, when the material still has its initial strength, the load capacity of the press fit is relatively high. Over time, creep (relaxation) also occurs at the macro level, which reduces the spring action and contact pressure. As a result, the friction coefficient and the load capacity of the entire press fit are strongly reduced.

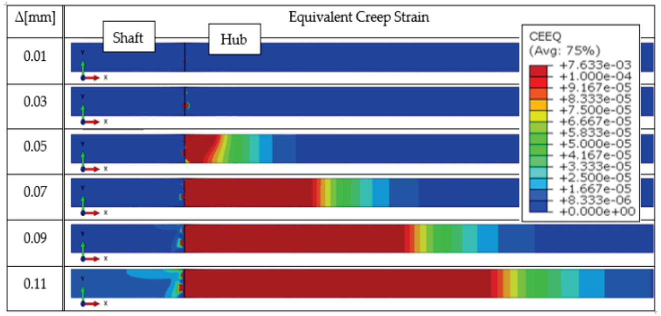

Figure 15 An equivalent creep strain in dependence on interference

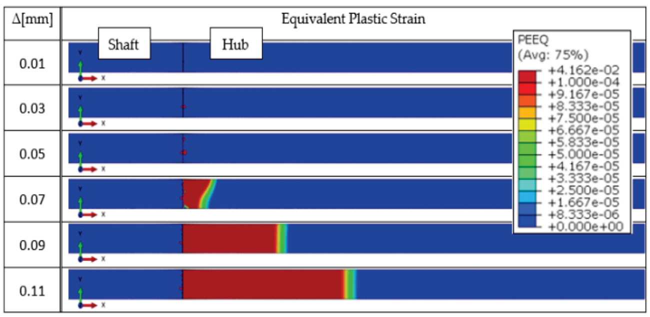

Figure 16 An equivalent plastic strain in dependence on interference

7 CONCLUSIONS

The study demonstrates that the loading capacity of a press fit is significantly affected by time-changing material and interference at used material and surface roughness. Experimental results have shown that the loading capacity increases with increasing interference up to a critical point, above which excessive plastic deformation at the macro level, over 1.6 ‰, reduces the strength of the joint. At a smaller interference, when plasticization is located only at the peaks of the rough surface at the micro level, over time, creep of the material causes the formation of a larger actual contact surface, increasing the coefficient of friction and thus the loading capacity of the press fit. At a larger interference, over 1.6 ‰, plasticization penetrates deeper into the material at the macro level. This causes stronger creep, which causes the contact pressure and coefficient of friction to drop; the press fit loses its original loading capacity.

Numerical simulation at a model of a rough contact surface confirms that the use of computational models based on the material elasticity and simpl Coulon's friction law, is not sufficient. For a deeper understanding of the process, it is necessary to use the visco-plastic behaviour of the material on a real rough contact surface. It turns out that it is more appropriate to use a friction model that takes in to account material cohesion and the formation of contact bridges. The results and findings show that at used material and surface roughness, it is also necessary to choose an appropriate oversize interference, if we want to produce a time-reliable and stiff joint.

The usual approach to calculating press fit in engineering practice uses the traditional Coulomb sliding friction model, where the sliding friction coefficient is more or less constant $\mu_0 \approx 0.2$. A solution approach is given based on a visco-plastic material and a more complex friction model; $\mu_0 \approx 0.6$. The results presented are valid for the used material and surface roughness. If we want to give a comprehensive recommendation for engineering use, it would be necessary to carry out a series of studies using different engineering materials and different combinations of surface roughness.

Acknowledgments

The authors acknowledge the Slovenian Research Agency ARIS for funding the Research Program P2-0137 "Numerical and experimental analysis of nonlinear mechanical systems".

8 REFERENCES

[1] Lewis, R., Marshall, M. B. & Dwyer-Joyce, R. S. (2005). Measurement of interface pressure in interference fits. *Proceedings of the Institution of Mechanical Engineers, Part C: Journal of Mechanical Engineering Science, 219*(2), 127-139. https://doi.org/10.1243/095440605X8432

[2] Madej, J. (2018). A strength analysis of the interference-fit joints. *Mechanik*, **91**(11), 1032-1034. https://doi.org/10.17814/mechanik.2018.11.185

[3] Stamenković, D., Milošević, M., Mijajlović, M. & Banic, M. (2011). Estimation of the static friction coefficient for press fit joints. *Journal of the Balkan Tribological Association, 17*(3), 341-355. https://www.researchgate.net/publication/241688933

[4] Persson, B.N.J. (2023). Influence of Surface Roughness on Press Fits. *Tribology Letters, 71*(19). https://doi.org/10.1007/s11249-022-01688-y

[5] Croccolo, D., De Agostinis, M. & Vincenzi, N. (2011). How to improve static and fatigue strength in press-fitted joints using anaerobic adhesive. *Proceedings of the Institution of Mechanical Engineers, Part C. Journal of Mechanical Engineering Science, 225*(12), 2792-2803. https://doi.org/10.1177/0954406211411402

[6] Kim, S. S. & Lee, D. G. (2006). Design of the hybrid composite bearing assembled by interference fit. *Composite Structures, 75*(1-4), 222-230. https://doi.org/10.1016/j.compstruct.2006.04.026

[7] Croccolo, D., Agostinis, M. D. & Vincenzi, N. (2012). Design of hybrid steel-composite interference fitted and adhesively bonded connections. *International Journal of Adhesion and Adhesives, 37*, 19-25. https://doi.org/10.1016/j.ijadhadh.2012.01.011

[8] Mori, K., Bay, N., Fratini, L., Micari, F. & Tekkaya, A. E. (2013). Joining by plastic deformation. *CIRP Annals – Manufacturing Technology, 62*(2), 673-694. https://doi.org/10.1016/j.cirp.2013.05.004

[9] Yang, G. M., Coquille, J. C., Fontaine, J. F. & Lambertin, M. (2001). Influence of roughness on characteristics of tight interference fit of a shaft and a hub. *International Journal of Solids and Structures, 38*(42-43), 7691-7701. https://doi.org/10.1016/S0020-7683(01)00035-X

[10] Zhang, Y., McClain, B. & Fang, X. (2000). Design of interference fits via finite element method. *International Journal of Mechanical Sciences, 42*(9), 1835-1850. https://doi.org/10.1016/S0020-7403(99)00072-7

[11] Lippmann, H. (1992). The effect of a temperature cycle on the stress distribution in a shrink fit. *International Journal of Plasticity*, (1), 567-582. https://doi.org/10.1016/0749-6419(92)90031-7
[12] Wang, G. S. (1994). Stress analysis for a lug under various conditions. *The Journal of Strain Analysis for Engineering Design, 29*(1), 7-16. https://doi.org/10.1243/03093247V291007
[13] Rudnytskyj, A. (2018). Simulations of contact mechanics and wear of linearly reciprocating block-on-flat sliding test. *Mechanical Engineering, master level, Lulea University of Technology, department of Engineering Sciences and Mathematics*. https://www.divaportal.org/smash/record.jsf?pid=diva2%3A1242768&dswid=7465
[14] Popov, V. L. (2010). Contact Mechanics and Friction. *Springer-Verlag Berlin Heidelberg*. https://doi.org/10.1007/978-3-642-10803-7
[15] Vukelic D., Prica M., Ivanov V., Jovicic G., Budak I. & Luzanin O. (2022). Optimization of Surface Roughness Based on Turning Parameters and Insert Geometry. *Int. Journal of Simulation Modelling, 21*(3), 417-428. https://doi.org/10.2507/IJSIMM21-3-607
[16] Milošević, A., Simunovic, G., Kanović, Ž., Simunovic, K., Santosi, Z., Šokac, M. & Vukelić, D. (2024). Comprehensive Evaluation of Dimensional Deviation, Flank Wear, SurfaceRoughness and Material Remuval Rate in Dry Turningof C45. *Steel Facta Universitatis, Series: Mechanical Engineering, 22*(4), 547-566. https://doi.org/10.22190/FUME240403024M
[17] Bowden, F. P. & Tabor, D. (2001). The Friction and Lubrication of Solids. *Clarendon Press, Oxford*.
[18] Decker, K.-H. (2024). Maschinenelemente. *Carl Hanser Verlag München Wien.*
[19] Nieman, G. (1981). Maschinen-elemente Band I Konstruktion und Berechnung von Verbindungen, Lagern, Wellen, *Springer-Verlag Berlin Heidleberg GmbH*.

Authors' contacts:

Vinko Močilnik, Assist. Prof. Dr.
University of Maribor, Faculty of Mechanical Engineering
Smetanova 17, 2000 Maribor, Slovenia
+386 31-331-664, vinko.mocilnik@gmail.com

Nenad Gubeljak, Full Prof. Dr.
(Corresponding author)
University of Maribor, Faculty of Mechanical Engineering
Smetanova 17, 2000 Maribor, Slovenia
+386 31 659 279, nenad.gubeljak@um.si

Jožef Predan, Assoc. Prof. Dr.
University of Maribor, Faculty of Mechanical Engineering
Smetanova 17, 2000 Maribor, Slovenia
+386 41 333 701, jozef.predan@um.si